Calcium oscillations in rhythmically active respiratory neurones in the brainstem of the mouse

Detlev Frermann, Bernhard U. Keller and Diethelm W. Richter

Zentrum Physiologie und Pathophysiologie, Universität Göttingen, Humboldtallee 23, 37073 Göttingen, Germany

(Received 9 April 1998; accepted after revision 21 October 1998)

1. The rhythmically active respiratory network in the brainstem slice of the mouse was investigated under *in vitro* conditions using patch clamp and microfluorometric techniques. Rhythmic respiratory activity persisted over the whole course of an experiment.

2. Electrophysiologically recorded rhythmic activity in respiratory neurones was accompanied by oscillations in intracellular calcium, which displayed a maximal concentration of 300 nM and decayed to basal levels with a mean time constant of $1{\cdot}6 \pm 0{\cdot}9$ s.

3. Elevations of calcium concentrations were highly correlated with the amplitude of rhythmic membrane depolarization of neurones, indicating that they were initiated by a calcium influx across the plasma membrane through voltage-gated calcium channels.

4. Voltage clamp protocols activating either high voltage-activated (HVA) or both HVA and low voltage-activated (LVA) calcium channels showed that intracellular calcium responses were mainly evoked by calcium currents through HVA channels.

5. Somatic calcium signals depended linearly on transmembrane calcium fluxes, suggesting that calcium-induced calcium release did not substantially contribute to the response.

6. For calcium elevations below 1 μM, decay time constants were essentially independent of the amplitude of calcium rises, indicating that calcium extrusion was adequately approximated by a linear extrusion mechanism.

7. Cytosolic calcium oscillations observed in neurones of the ventral respiratory group provide further evidence for rhythmic activation of calcium-dependent conductances or second messenger systems participating in the generation and modulation of rhythmic activity in the central nervous system.

In the central nervous system, defined neuronal networks generate rhythmic activity controlling locomotion, respiration, swallowing and other basic physiological functions. The network generating rhythmic respiratory activity in mammals represents an important model system for studying the principles of generation and modulation of rhythmic activity in general, allowing electrophysiological measurements of rhythmic activity even in isolated slice preparations *in vitro* (see for example Smith *et al.* 1991, 1992; Onimaru & Homma, 1992; for review see Richter *et al.* 1992). In such measurements, all neuronal elements necessary to control rhythmic respiratory movements have been identified in the lower brainstem (Smith *et al.* 1991; Bianchi *et al.* 1995). Further electrophysiological and anatomical studies have identified the ventral respiratory group (VRG), especially the pre-Bötzinger complex, as the primary locus where the respiratory rhythm is generated (Smith *et al.* 1991; Ramirez *et al.* 1996). In mammals, generation of the respiratory rhythm results from a co-ordinated pattern of neuronal activity involving synaptic events, membrane conductances and their modulation by intracellular second messenger systems (Richter *et al.* 1992; Champagnat & Richter, 1993).

Functional and pharmacological analysis of VRG neurones has suggested that excitatory synaptic activity and corresponding changes in intracellular calcium concentrations may play an important role in generation and/or modulation of rhythmic respiratory activity (Richter *et al.* 1993; Pierrefiche *et al.* 1995). Excitatory synaptic transmission in VRG neurones is primarily mediated by glutamatergic synapses, and both AMPA and NMDA receptor channel types are involved in synchronizing rhythmic respiratory events (Greer *et al.* 1991). Although the functional role of specific glutamate receptor types is as yet unclear, periodic membrane depolarizations provide favourable conditions for NMDA receptor activation and the development of bursts of action potential discharges that induce postsynaptic calcium influx (Foutz *et al.* 1989; Greer *et al.* 1991; Funk *et al.* 1993). In addition, other calcium-dependent conductances seem to be involved in respiratory

rhythm generation. For example, repolarization of membrane potential after repetitive action potential discharges is retarded when changes in intracellular calcium concentrations are suppressed by elevated cytosolic calcium buffering (Richter *et al.* 1993; Pierrefiche *et al.* 1995), suggesting a functional role of calcium elevations in controlling calcium-activated potassium efflux and membrane repolarization during ongoing rhythmic activity.

Under resting conditions, intracellular calcium concentrations are commonly determined by multiple processes including calcium extrusion across the plasma membrane via Na^+–Ca^{2+} exchangers, Ca^{2+}-ATPases, Ca^{2+} sequestration, Ca^{2+} uptake in organelles and Ca^{2+} buffering. Transient elevations of intracellular calcium might occur as a result of calcium influx through voltage-operated Ca^{2+} channels, receptor-operated channels and a variety of calcium release mechanisms from intracellular stores (Onimaru *et al.* 1996; Fierro & Llano, 1996; Bootman *et al.* 1997). Different types of voltage-operated calcium channels have been described in neurones which differ in their basic functional properties, like voltage dependence and ion selectivity, and in their pharmacological profile (Carbone & Lux, 1987; Tsien & Tsien, 1990; Pietrobon *et al.* 1990; Penner *et al.* 1993; Pierrefiche *et al.* 1995; Onimaru *et al.* 1996). Four major classes of calcium channels, defined as T-type, L-type, N-type and P/Q-type, have been shown to exist in brainstem neurones. Their role in generating and modulating rhythmic respiratory activity has been investigated by utilizing subtype-specific pharmacological tools such as nifedipine, ω-conotoxin, ω-agatoxin, verapamil and other calcium channel blockers (Tsien & Tsien, 1990; Pietrobon *et al.* 1990; Richter *et al.* 1993; Viana *et al.* 1993; Pierrefiche *et al.* 1995; Onimaru *et al.* 1996). With respect to their voltage dependence, they are commonly divided into two major groups defined as high-voltage activated (HVA) and low-voltage activated (LVA) channels (Bertolino & Llinas, 1992; Richter *et al.* 1993; Pierrefiche *et al.* 1995; Onimaru *et al.* 1996). Although calcium influx through both types has been observed in respiratory neurones, the precise subcellular pattern of calcium influx through either LVA or HVA channels remains to be determined.

The aim of this study is to investigate the dynamics of intracellular calcium concentrations during spontaneous rhythmic respiratory activity. We recorded electrical activity and simultaneously measured intracellular calcium concentrations in identified neurones in the functionally intact respiratory network *in situ*. Our results show that intracellular calcium concentrations oscillate significantly during ongoing rhythmic activity, suggesting that rhythmic activation of calcium-dependent ion conductances and second messenger systems might modulate respiratory activity in the mammalian central nervous system. In addition, we investigated calcium influx pathways controlling calcium oscillations by using defined voltage clamp protocols. Some results have been published in preliminary form (Frermann *et al.* 1997*a*, *b*).

METHODS

Slice preparation and electrophysiological recording

To analyse the calcium transients of rhythmically active neurones from the respiratory-related network of the pre-Bötzinger complex, NMR-1 mice at an age of 2–8 days were anaesthetized in a chamber containing an ether vapour-enriched atmosphere, and were immediately decapitated. The experiments were carried out in accordance with the guidelines of the Ethics Committee of the Medical Faculty of the University of Göttingen. The brain was removed in cold artificial cerebrospinal fluid (ACSF; 118 mM NaCl, 3 mM KCl, 1 mM $MgCl_2$, 25 mM $NaHCO_3$, 1 mM NaH_2PO_4, 1·5 mM $CaCl_2$, 30 mM glucose), which was continuously bubbled with carbogen (95% O_2, 5% CO_2). The brainstem was isolated, fixed to an agar block and mounted in an upright position with the rostral side upwards and the dorsal side facing the slicer blade. The brainstem and agar block were inclined 20 deg in the dorsal direction. In cold ACSF a 700 μm thick slice located rostral to the edge of the area postrema was cut. Topographic 'landmarks' including the facial nucleus, inferior olive (IO), nucleus of the solitary tract (NTS), hypoglossal nucleus (XII) and the nucleus ambiguus (NA) were used to yield a reproducible cutting plane. Slices contained the pre-Bötzinger complex, the network known to generate respiratory rhythms *in vivo*, as well as the hypoglossal (XII) nerve activity (Ramirez *et al.* 1996). For a 30 min recovery period, the slice was maintained at 29–30 °C in continuously carbogen-bubbled bicarbonate-buffered saline solution at pH 7·4. Afterwards slices were transferred to the recording chamber, fixed in the chamber rostral side upwards with a nylon net under an upright microscope (Zeiss) and continuously superfused with ACSF (up to 20 ml min^{-1}). Respiratory rhythmic activity was identified by extracellular suction electrode recordings of hypoglossus nerve rootlet (XII) activity. The potassium concentration in the bath solution was gradually raised to concentrations of 6–8 mM to maintain the respiratory rhythm as previously reported (Smith *et al.* 1991; Ramirez *et al.* 1996).

By using infrared differential interference contrast optics (IR-DIC; Stuart *et al.* 1993; Dodt & Zieglgänsberger, 1994) individual cells could be visualized by suitable video equipment. Depending on the age of the animal, cells up to a depth of approximately 100 μm below the slice surface could be visualized. Rhythmically active neurones located within the pre-Bötzinger complex and near or in the nucleus ambiguus (Fig. 1) were patch clamped according to previously described techniques (Hamill *et al.* 1981; Sakmann *et al.* 1989; Keller *et al.* 1991; Titz & Keller, 1997; Weigand & Keller, 1998) and fura-2 loaded to monitor calcium transients. Extracellular recordings from hypoglossal rootlets were obtained along with intracellular recordings from rhythmically active respiratory neurones. All chemicals were purchased from Sigma, except fura-2 (potassium salt), which was obtained from Molecular Probes.

Electrophysiological measurements

Suction electrodes as well as patch pipettes were pulled from borosilicate glass tubing (Kimble Glass Inc, Vineland, NJ, USA) and fire polished before use. Suction electrodes were filled with ACSF and had diameters of approximately 50–80 μm to get a tight connection between rootlet and pipette. Extracellular recordings were rectified, low pass filtered and integrated (Fig. 2). Spires of patch pipettes had diameters of 1–2 μm and resistances of 2·5–4·5 MΩ when filled with standard intracellular solution (160 mM KCl or potassium D-gluconate, 2·2 mM $MgCl_2$, 11 mM Hepes, 4·4 mM ATP and 0·44 mM GTP). Pipette solutions additionally contained fura-2 concentrations ranging from 20 to

200 μM. Respiratory neurones were identified by their firing pattern, which was strictly correlated with XII nerve activity; their somatic diameters, which appeared in our slicing plain to be below 18 μm; a compact dendritic tree; and their localization in and ventrolateral to the nucleus ambiguus (Fig. 1). Pipettes could be moved (piezo-driven) in three directions allowing stable whole-cell patch clamp recordings from visually identified neurones situated close to the surface of the slice. Currents were recorded with sampling frequencies of 5 kHz and filtered as indicated in the figure legends. The series resistance (R_s) of neurones before compensation was typically 8–15 MΩ. Recordings with series resistances above 15 MΩ were not further analysed. Values of R_s and membrane capacitance (C_m) were obtained from settings of the capacitance compensation circuitry of the patch clamp amplifier and monitored during the experiment. Usually a series resistance compensation of 60% was employed. Cells were examined in voltage clamp and current clamp whole-cell mode using an EPC 7 amplifier (List Medical).

Microfluorometric measurements

Neurones were loaded via the patch pipette using solutions containing 50–200 μM of the calcium indicator dye fura-2. The dye was excited at 360 and 380 nm for calcium-independent and calcium-dependent fluorescence measurements, respectively, by either using a rotating filter wheel device (Fig. 4) or a computer-controlled monochromator (TILL Photonics, Planegg, Germany) that permitted switching between different excitation wavelengths within 5 ms (Keller *et al.* 1992; Lips & Keller, 1998). The emission wavelength (500–530 nm) of the dye was monitored using a 'view finder' system (TILL Photonics) in conjunction with a photomultiplier. Regions of interest (ROI) over the cell body of single respiratory neurones were chosen during a patch clamp experiment (Fig. 1*B*). Rapid calcium measurements with a sampling interval of 1·5 ms were performed at constant excitation wavelengths of 380 nm during short stops of the filter wheel (Fig. 3). Calcium concentrations were determined according to the equation:

$$[Ca^{2+}]_i = K_{eff}^* (R - R_{min})/(R_{max} - R),$$

where R denotes the fluorescence ratio F_{360}/F_{380} according to Grynkiewicz *et al.* (1985). Calibration constants R_{min}, R_{max} and K_{eff} were regularly determined during *in situ* calibrations (Neher & Augustine, 1992; Zhou & Neher 1993; Schneggenburger *et al.* 1993; Neher, 1995; Fierro & Llano, 1996; Helmchen *et al.* 1996; Lips & Keller, 1998). Typical values were $R_{min} = 0{\cdot}03$, $R_{max} = 0{\cdot}25$ and $K_{eff} = 1200$ nM for the filter wheel device.

Data analysis

Patch clamp recordings and microfluorometric measurements were analysed using a semi-automated software package run on a Macintosh Power PC (PULSEFIT, HEKA Electronik, Lambrecht/Pfalz, Germany). Rise times of calcium transients were measured using the integrated signal of one cell and defined as the time from 20 to 80% of the amplitude. The decay time constant of calcium transients was determined by a single exponential fit from peak to baseline. Electrophysiological data were bandpass filtered as indicated to reduce noise. Values are given throughout the text as means ± S.D.

RESULTS

Rhythmically active neurones located in the pre-Bötzinger complex were patch clamped and filled with the calcium-sensitive indicator dye fura-2. Respiratory neurones with round to ellipsoid cell bodies with an average apparent diameter of 16 μm were identified by their characteristic pattern of action potential discharges ('bursts') that occurred time locked with respiratory bursts recorded from the rootlet of hypoglossal nerves (XII nerve; Fig. 1*A*). They could be visually identified in slices with a thickness up to 700 μm in and ventrolateral to the pars compacta of the nucleus ambiguus by using infrared differential interference contrast optics as described by Stuart *et al.* (1993; Fig. 1*B*). Summation potentials of hypoglossal nerve activity (Fig. 2) were monitored during patch clamp experiments as previously described (Smith *et al.* 1991; Funk *et al.* 1993; Lips & Keller, 1998). The mean interval between bursts of hypoglossal nerve activity was 8·4 ± 4·4 s ($n = 64$; 28 °C) and the mean burst length was 815 ± 170 ms ($n = 50$).

Intracellular recordings were performed on 96 neurones by using standard equipment for patch clamp measurements in brain slices (Hamill *et al.* 1981; Edwards *et al.* 1989; Titz & Keller, 1997; Lips & Keller, 1998). After establishing the whole-cell configuration, electrical activity of inspiratory neurones was monitored in voltage and current clamp modes. Neuronal resting potentials were found between −60 and −70 mV ($n = 7$) and rhythmic electrical signals were time locked with hypoglossal nerve activity (Fig. 2*B* and *C*). The subpopulation of inspiratory active neurones investigated displayed input resistances ranging from 600 to 800 MΩ separating them functionally from vagal motoneurones also located in the nucleus ambiguus, which are known to display lower input resistances of around 120 MΩ (Rekling *et al.* 1996; Rekling & Feldman, 1997). Complete current–voltage relationships of inspiratory interneurones are illustrated in Fig. 3. They showed no (Fig. 3*A*) or little (Fig. 3*B*) action potential activity during depolarizing voltage ramps and displayed a notable outward rectification for voltages positive to −20 mV. This also distinguished them from vagal motoneurones which displayed sustained action potential activity during depolarizations and linear current–voltage relationships (Rekling *et al.* 1996; Rekling & Feldman, 1997).

During patch clamp recordings cells were loaded via the pipette with a concentration of between 50 and 200 μM fura-2, allowing us to perform measurements of somatic calcium transients within the first few seconds after establishing the whole-cell configuration. Alternating excitation wavelengths for ratiometric calcium measurements (360 nm, 380 nm; Grynkiewicz *et al.* 1985) were achieved either by a rotating filter wheel in the excitation pathway (Fig. 4) or a computer-controlled monochromator that permitted changes between 360 and 380 nm excitation wavelengths within 5 ms for rapid calcium measurements. The emission signal of fura-2 was integrated over a rectangular window on the somatic surface of 18 μm × 18 μm in size (Fig. 1*B*) and collected by a photomultiplier. Experimental conditions were sufficiently stable to perform patch clamp measurements over several hours from a single slice.

Simultaneous patch clamp and microfluorometric recordings of rhythmically active respiratory neurones are illustrated

in Fig. 5. All neurones showed phase-locked inspiratory activity with rhythmic output of the hypoglossal nerve. In current clamp recordings, respiratory discharges ('bursts') were apparent as spontaneous, periodic membrane depolarizations starting from a resting potential of −70 mV (mean, −71 ± 8 mV, $n = 6$) leading to repetitive discharge of action potentials. Periodic membrane depolarizations had mean amplitudes of 24 ± 5 mV ($n = 6$; Fig. 5) and led to burst discharges that lasted over several hundred milliseconds (mean, 408 ± 158 ms, $n = 6$). Depolarizations were accompanied by rapid rises of intracellular calcium concentrations as illustrated in Fig. 5*A*. Calcium elevations were clearly detectable in the soma during rhythmic discharges of action potentials. Maximum elevations of intracellular calcium varied significantly between different bursts and cells, with a maximum amplitude of 300 nM (mean, 212 ± 85 nM, $n = 7$) above resting concentrations (mean, 120 ± 70 nM, $n = 7$) for spontaneous events. Even single action potentials were sufficient to induce detectable calcium responses as illustrated in Fig. 5*B*. In this case, calcium amplitudes were small compared with long-lasting bursts but the kinetic profiles were similar. Mean rise time of burst-related calcium transients was 151 ± 95 ms as determined from a linear fit to the rising phase of signals (Fig. 6; $n = 7$ cells, 20–80 % maximum amplitude).

Calcium decay times also showed a broad diversity, but they were usually well approximated by a single exponential function as illustrated in Fig. 6 (mean decay = 1·6 ± 0·9 s; $n = 6$). A heterogeneity in decay time constants was

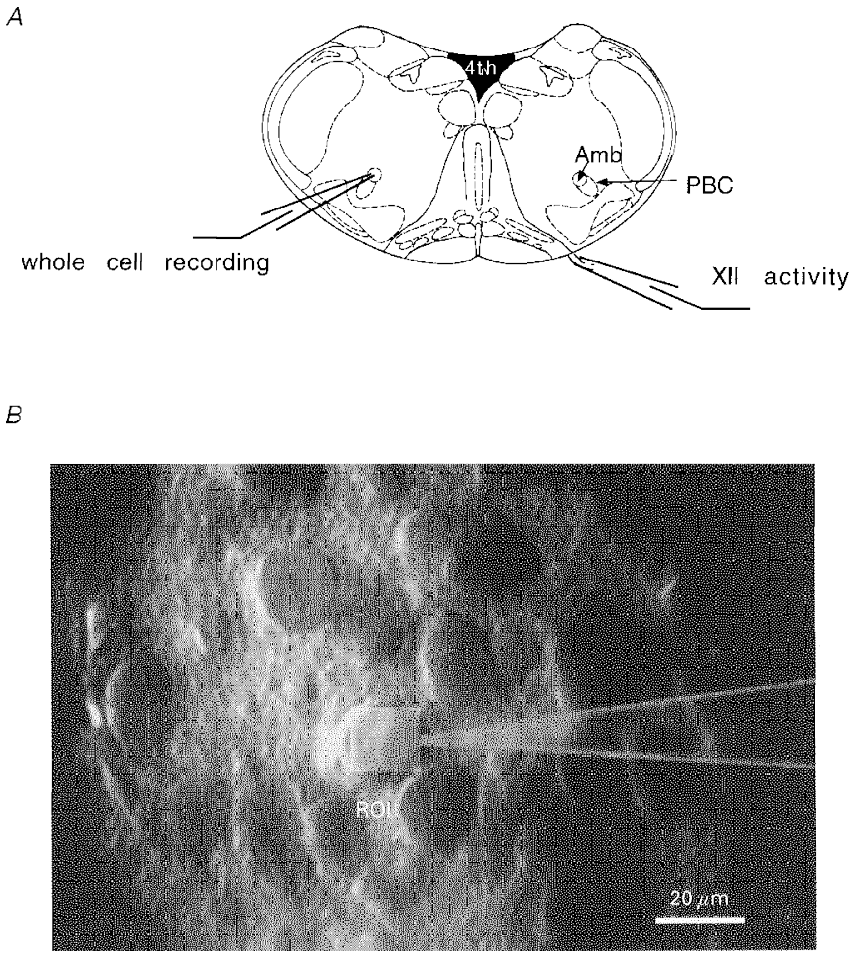

Figure 1. Brainstem slice preparation of the medulla oblongata

Schematic representation of a transverse brainstem slice and respiratory cells visualized in a thick slice with a schematic pipette and region of interest (ROI). *A*, respiratory rhythms were recorded from the hypoglossus nerve with a suction electrode. Either ipsilateral or contralateral patch clamp experiments were performed in the ventral respiratory group and especially the Pre-Bötzinger complex in the region of the nucleus ambiguus. *B*, cells were patch clamped under visual control using IR illumination in an upright microscope. After fura-2 loading of cells, fluorescence signals were recorded by photomultiplier detection integrating the fluorescence over a rectangular region of interest adjusted to cover the soma of the cell (light rectangle). During an experiment, size and location of the detection window could be adjusted if necessary. PBC, pre-Bötzinger complex; Amb, nucleus ambiguus; XII, hypoglossus nerve; ROI, region of interest.

partially explained by differences in the fura-2 filling state of cells (Neher & Augustine, 1992; Helmchen *et al.* 1997; Lips & Keller, 1998), which could be experimentally monitored by calcium-independent fluorescence signals at 360 nm. The dependence of calcium decay time constants on fura-2 filling states is a useful parameter that – under appropriate experimental conditions – permits the determination of the endogenous calcium buffering conditions of the cell (Neher & Augustine, 1992; Helmchen *et al.* 1997; Lips & Keller, 1998). For the analysis of spontaneous calcium signals presented in this report, moderate fura-2 concentrations up to 200 μM were chosen to characterize respiratory-related calcium oscillations under close-to-physiological conditions.

Respiratory neurones were also studied in the voltage clamp mode to investigate the molecular processes underlying spontaneous calcium oscillations. Under voltage clamp conditions, rhythmic respiratory activity was represented by periodic synaptic currents with average amplitudes of 422 ± 153 pA ($n = 10$; Fig. 7). Calcium oscillations were absent when the resting membrane potential was held constant at a level of −70 mV. This indicated that calcium influx as measured in current clamp mode was critically dependent on depolarizations of the soma. To further define the role of voltage-dependent calcium influx pathways, we performed a series of experiments based on defined voltage step protocols. Figure 8 illustrates recordings of membrane currents and intracellular calcium concentrations during a

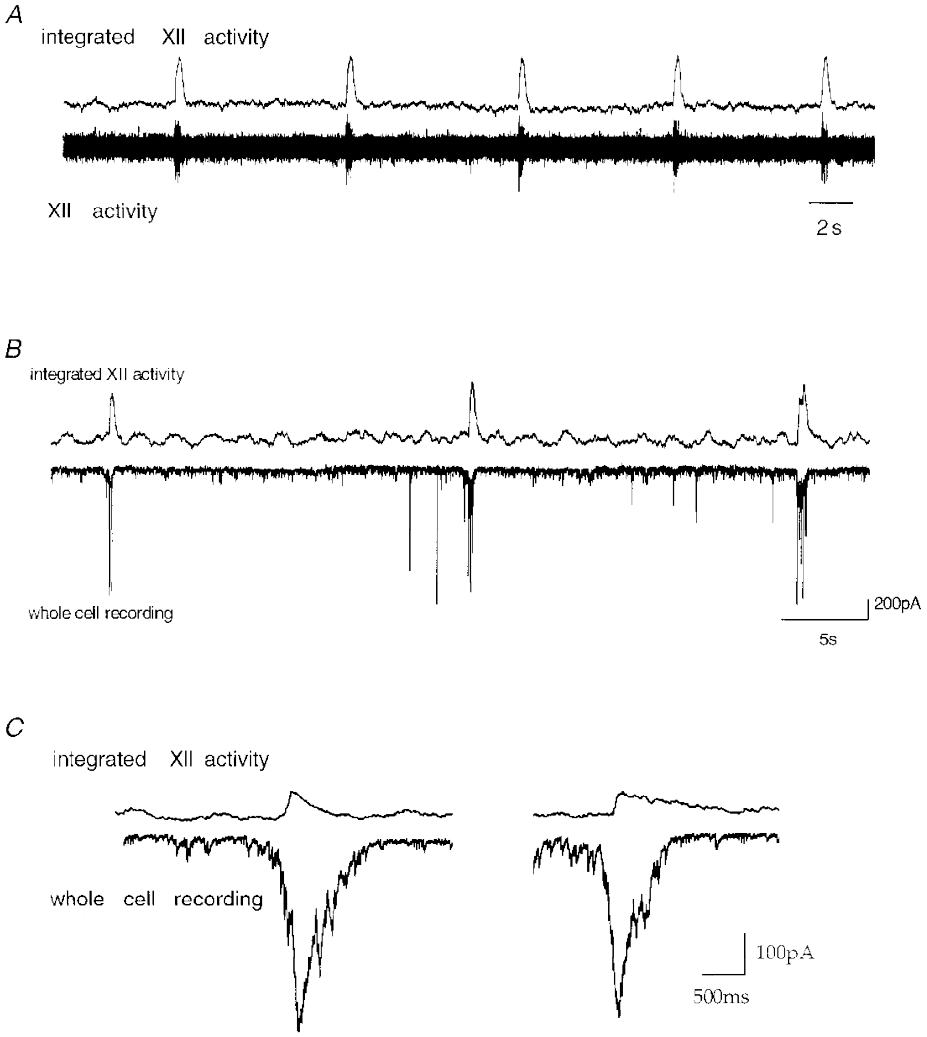

Figure 2. Simultaneous recording of hypoglossal nerve activity and neuronal activity in respiratory neurones

Spontaneous rhythmic activity of single neurones and the output of the network are displayed. Upper traces in *A–C* all depict integrated hypoglossal (XII) nerve rootlet activity. *A*, lower trace, recording of hypoglossal nerve rootlet activity. *B*, lower trace, a voltage patch clamp recording from a neurone of the pre-Bötzinger complex at a holding potential of −70 mV. Neuronal currents are in phase with XII rootlet activity. *C*, integrated XII rootlet activity and inward current of respiratory neurones at expanded time scale.

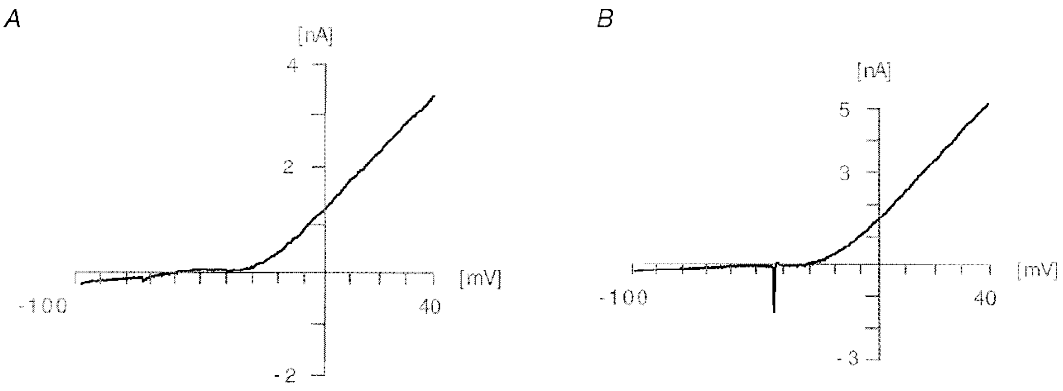

Figure 3. Relationship between membrane potential and injected current in respiratory active neurones of the pre-Bötzinger complex

The figure shows the parameters of the voltage ramp (−100 to 40 mV, 200 mV s^{-1}) performed to investigate the *I–V* relationship. The majority of the examined neurones showed *I–V* relationships as depicted in *A* with a pronounced inward rectification negative to −20 mV and a linear relationship positive to −20 mV. In some cases action potentials were evoked (*B*).

voltage clamp experiment in which the membrane voltage was held at −70 mV and depolarized in consecutive command voltage steps of +10 mV. Depolarization-induced net current signals were directed outward, and are most likely to reflect an efflux of potassium ions across the plasma membrane. Simultaneous fluorescence measurements revealed a significant increase in intracellular calcium concentrations even when there was no net inward cation current detectable. Figure 8*B* illustrates this in more detail by showing the rise in intracellular calcium concentration as a function of membrane potential during depolarizing voltage commands. Somatic rises in $[Ca^{2+}]_i$ were already observed when the neurone was depolarized positive to −60 mV, a situation that frequently occurred during normal rhythmic respiratory activity (Fig. 5). Depolarizations to −50 mV or more evoked significant calcium responses with amplitudes that usually saturated around 0 mV. Half-maximum calcium responses were evoked by depolarizations to -40 ± 6 mV ($n = 16$ cells). Further depolarizations to voltages positive to +20 mV evoked saturating calcium responses where maximum amplitudes were most likely to be limited by the reduced driving force for calcium influx in the positive voltage range.

To differentiate between the contributions of low voltage-activated (LVA) and high voltage-activated (HVA) calcium channels, we first utilized a voltage protocol illustrated in Fig. 9*A*, where LVA channels were forced into inactivated states by holding the resting membrane potential at −70 mV (see also Carbone & Lux, 1987; Richter *et al.* 1993;

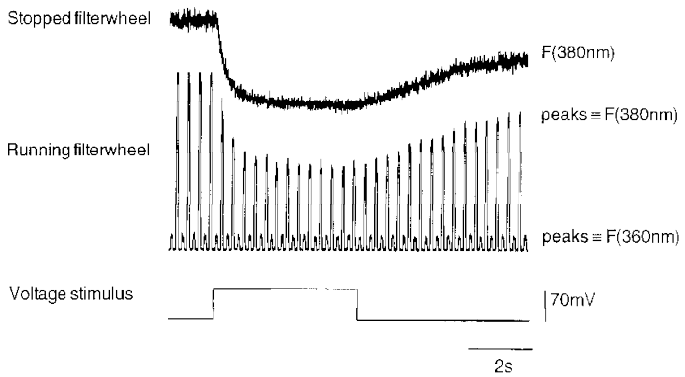

Figure 4. Basic principle of microfluorometric measurements

Fluorescence measurements during a depolarizing voltage step from −70 to 0 mV. During control recordings, fluorescence signals were measured by using a rotating filter wheel equipped with 360 and 380 nm bandpass filters (excitation wavelengths). Calcium-independent wavelength is represented by lower peaks and calcium-dependent wavelength by higher peaks. Note the stable amplitude of 360 nm signal during intracellular calcium change. For rapid calcium measurements, the filter wheel could be stopped and controlled independently for measurements at F_{360} or F_{380} only. The upper record shows F_{380} recorded in the same cell as the lower record.

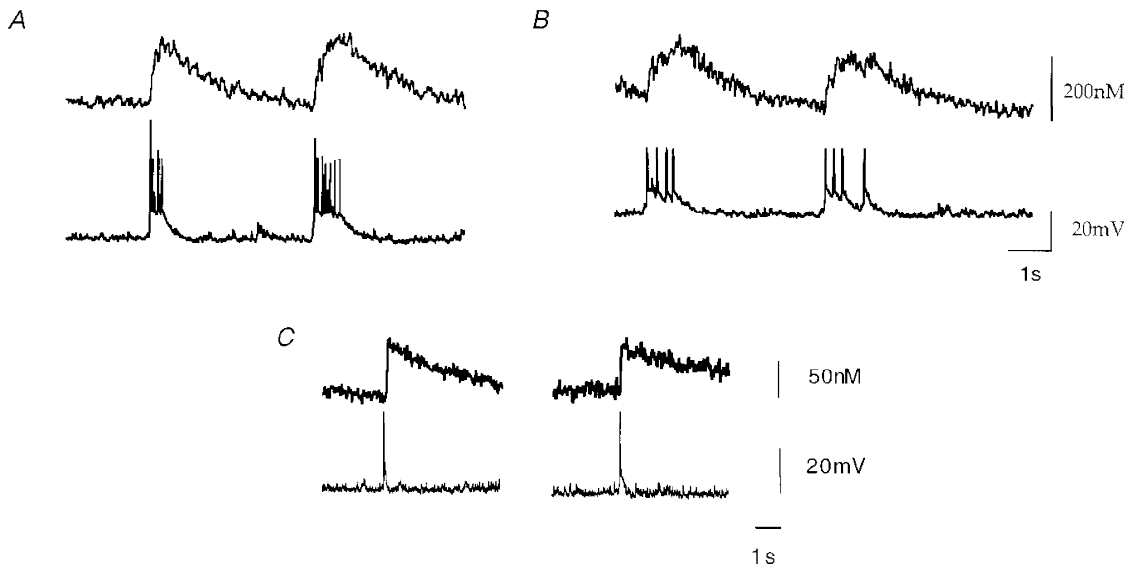

Figure 5. Simultaneous microfluorometric and current clamp patch recordings

A, rhythmic burst activity and intracellular calcium changes recorded from respiratory neurones in the whole-cell patch clamp configuration. Fast calcium signals (upper traces in *A* and *B*) were obtained by rapid sampling frequencies of F_{380} and low pass filtering at 100 Hz. After performing rapid recordings the filter wheel was again rotated to allow simultaneous measurements of F_{360} and F_{380} for off-line ratiometric analysis. *B*, intracellular calcium transients associated with a single action potential recorded in current clamp mode.

Pierrefiche *et al.* 1995; Onimaru *et al.* 1996). Somatic calcium responses were evoked by step-like depolarizations of the somatic membrane to voltages between −60 and +30 mV. Calcium responses were compared with those obtained after short hyperpolarizations to −90 mV (Fig. 9*B*), known to remove LVA channels from inactivated states. Interestingly, somatic responses evoked by both protocols were similar, suggesting that contributions of LVA channels were small compared with those of HVA channels under our experimental conditions. A quantitative analysis showed that amplitudes of calcium responses during both protocols differed by less than 6·3 ± 1·8% ($n = 3$ cells), confirming the qualitative observation.

One possible explanation for the absence of LVA channel-mediated signals is a 'rundown' of calcium responses between the two protocols. Several observations argued against this

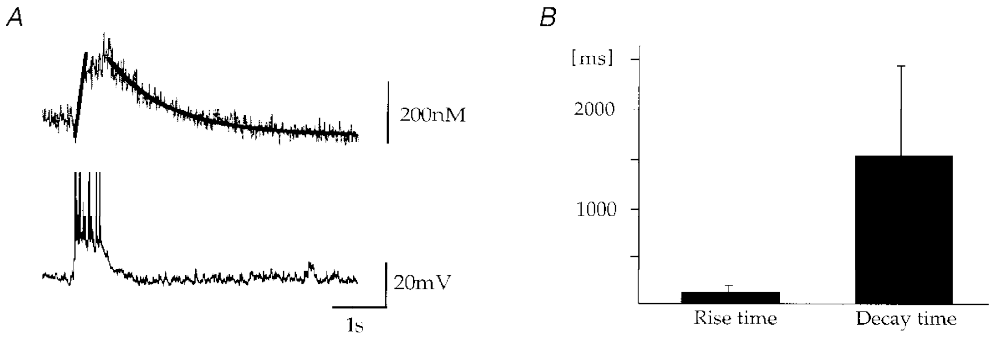

Figure 6. Kinetics of spontaneous calcium transients during rhythmic activity in CC

Rise times and decay times were measured with maximum intracellular fura concentrations of 200 μM. *A*, the upper trace represents the calcium transient elicited by spontaneous depolarization of the cell (bottom trace). The graph in the upper trace depicts the time course of calcium transients as fitted functions. Rise time of rising phase was determined by linear regression and determined as 180 ms (20–80% maximum amplitude) for the record shown. Decay times were determined by fitting a single exponential function to the calcium concentration (1·2 s for the record shown). *B*, average rise and decay time of calcium oscillations obtained from 7 neurones. The average rise time (20–80% maximum amplitude) was given by 151 ± 95 ms and the mean decay time for a single exponential fit was 1·6 ± 0·9 s. Note the significant variability for both parameters.

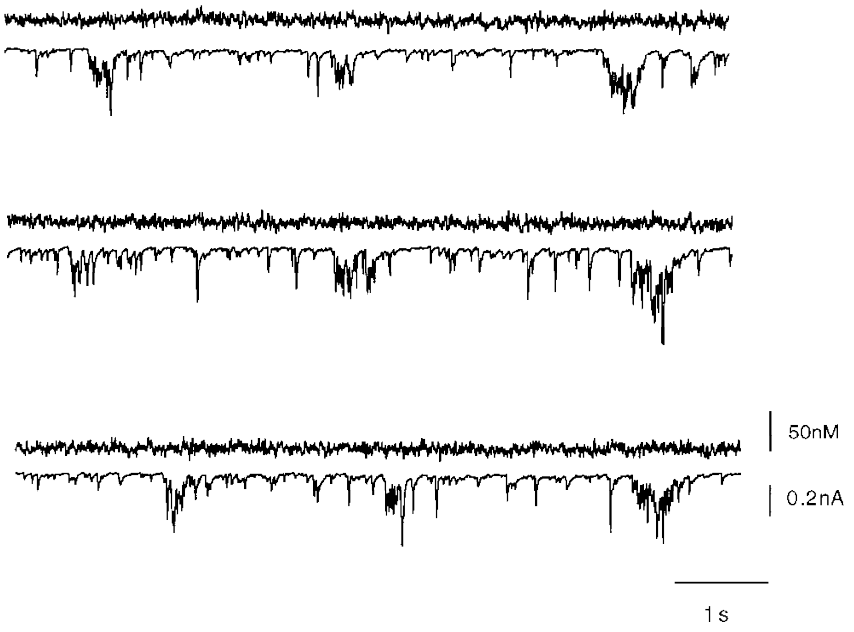

Figure 7. Intracellular calcium transients during voltage clamp measurements

Patch clamp recordings in voltage clamp mode during simultaneous microfluorometric calcium measurements of a rhythmically active respiratory neurone. Upper traces show the calcium signal measured with the dye fura-2. Bottom traces show the voltage clamp signal of rhythmic respiratory neurones. The somatic membrane potential was held at −70 mV. Even in those cases where the voltage clamp of the neurone was imperfect and action potentials were observed in voltage clamp mode no calcium transients could be detected. Calcium signals were recorded as described in Fig. 3. Whole-cell currents were sampled at 5 kHz.

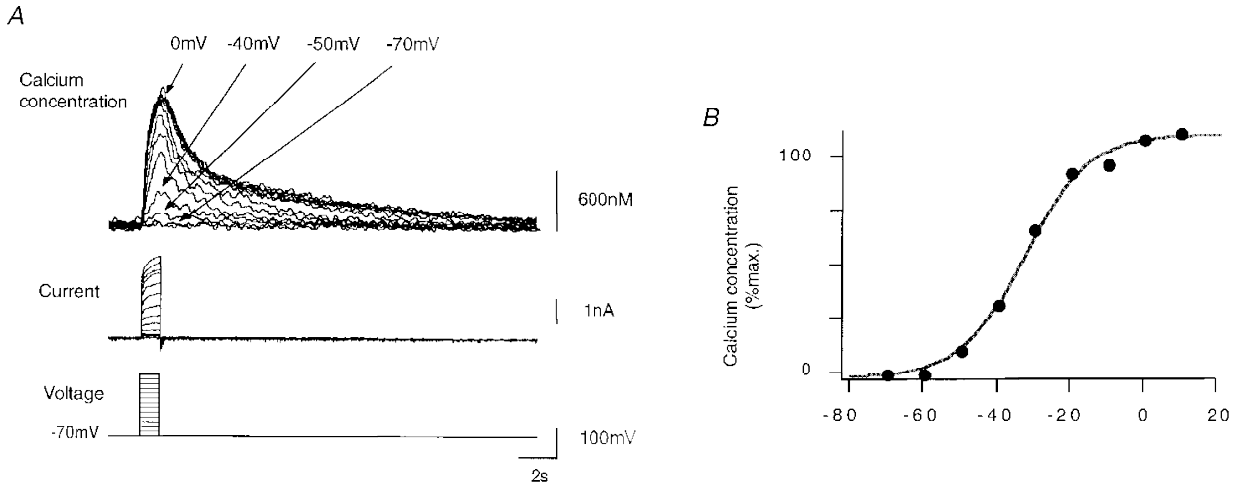

Figure 8. Intracellular calcium transients during depolarizing voltage steps

Calcium responses during voltage step protocols. During fura-2 loading, cells were clamped at −70 mV. *A*, somatic calcium was measured during voltage steps of +10 mV between −70 and +20 mV lasting 500 ms. F_{380} was monitored during the time interval of interest and calculation of fluorescence ratio F_{360}/F_{380} was performed off-line during data analysis. *B*, peak somatic calcium concentration during voltage step protocol. Note the significant elevation of calcium concentration for depolarized membrane potentials positive to −60 mV. The continuous line corresponds to the least square fit of the function $f(V) = 1/(1 + \exp(-a(V + V_m)))$ with parameters $a = 0{\cdot}11595$ mV^{-1} and $V_m = -33{\cdot}3$ mV.

possibility. First, somatic calcium responses were recorded directly after establishing the whole-cell configuration and compared with calcium signals evoked later by an identical protocol. Average results from five cells demonstrated that somatic calcium responses decreased by 17 ± 10 % in a time interval of 30 min. This was significantly longer than the time interval required for the protocols illustrated in Fig. 9 (7 min), arguing that rundown of calcium responses was not a dominant factor.

An important question is related to the potential contribution of calcium-induced calcium release to spontaneous calcium oscillations. To estimate the potential role, we measured rises in somatic $[Ca^{2+}]_i$ as a function of calcium influx. This was achieved by depolarizing the somatic membrane to voltages of 0 mV for time intervals lasting 5 ms, 10 ms, etc. up to 1000 ms. As illustrated in Fig. 10, long-lasting depolarizations were accompanied by higher elevations in intracellular calcium signals. Figure 10*B* shows the peak calcium concentration as a function of depolarization time interval. For intervals below 1000 ms and moderate elevations below 1 μM, somatic calcium concentrations showed a linear dependence on depolarization time ($n = 6$ cells). This indicated that calcium-induced calcium release, expected to lead to significant inhomogeneities during this protocol (Llano *et al.* 1994), did not dominate somatic signals under our conditions.

In a further series of experiments we investigated calcium extrusion mechanisms in respiratory neurones. This was done by monitoring the decay of calcium responses during depolarizing voltage steps of varying length. For elevations below 1 μM, decays of calcium signals were well approximated by a single exponential function (Fig. 11, $n = 20$ cells analysed). For inspiratory neurones, these results indicated that the combined action of calcium pumps and uptake could be effectively approximated by a linear kinetic scheme with calcium-independent rate constants. This was not valid for calcium elevations above 1 μM $[Ca^{2+}]_i$, which often decayed according to multiple exponential components (see for example Fig. 8*A*, top record), suggesting the involvement of additional regulatory processes with more complex kinetic properties. Also, calcium decay time constants showed little dependence on calcium amplitudes (Fig. 11*B*). Depolarizations to 0 mV for 50 and 1000 ms evoked calcium responses with mean decay time constants of $2{\cdot}4 \pm 1$ and $2{\cdot}6 \pm 1$ s, respectively ($n = 9$ cells). These time constants were not significantly different ($P < 5$ %, Student's unpaired t test).

DISCUSSION

In vitro preparations of functionally intact neuronal networks promise to serve as valuable tools for investigation of mechanisms generating and modulating neuronal activity in general (Smith *et al.* 1991; Smith *et al.* 1992; Onimaru &

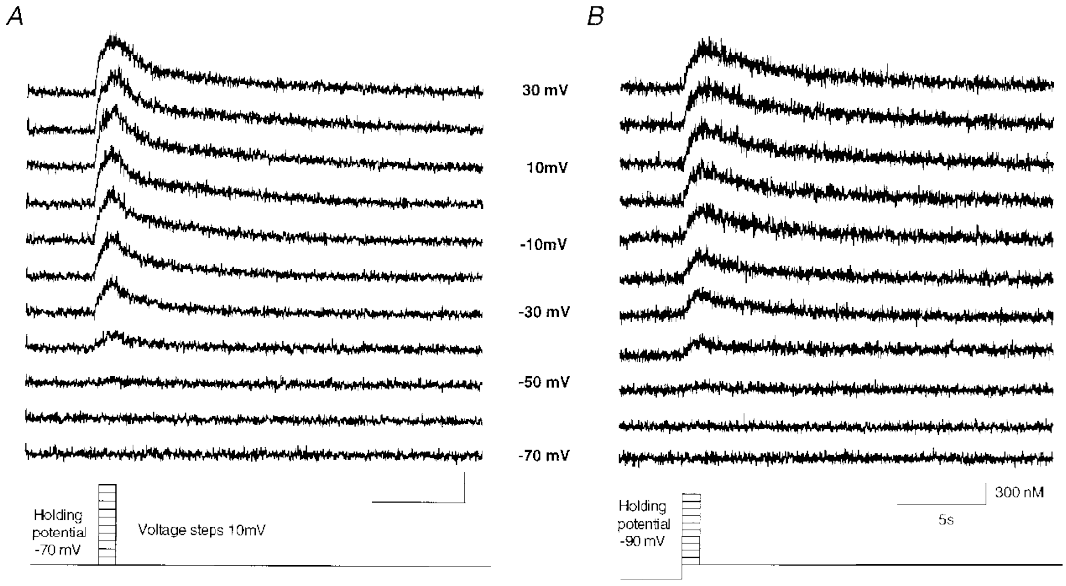

Figure 9. Intracellular calcium transients during depolarizing voltage steps related to HVA and LVA channels

Upper traces show calcium transients during different voltage step protocols depolarizing cells as shown at the bottom. *A*, a voltage clamped cell was depolarized from a holding potential of −70 mV in 10 mV steps to +30 mV. *B*, the calcium influx with a voltage step protocol depolarizing cells from a holding potential of −90 mV in 10 mV steps to +30 mV. *A* shows the $[Ca^{2+}]_i$ mediated from HVA channels whereas *B* shows $[Ca^{2+}]_i$ of HVA and LVA calcium channels. Low voltage-activated channels are most likely to be inactivated during this voltage clamp protocol. Calibration values for *A* are the same as in *B*.

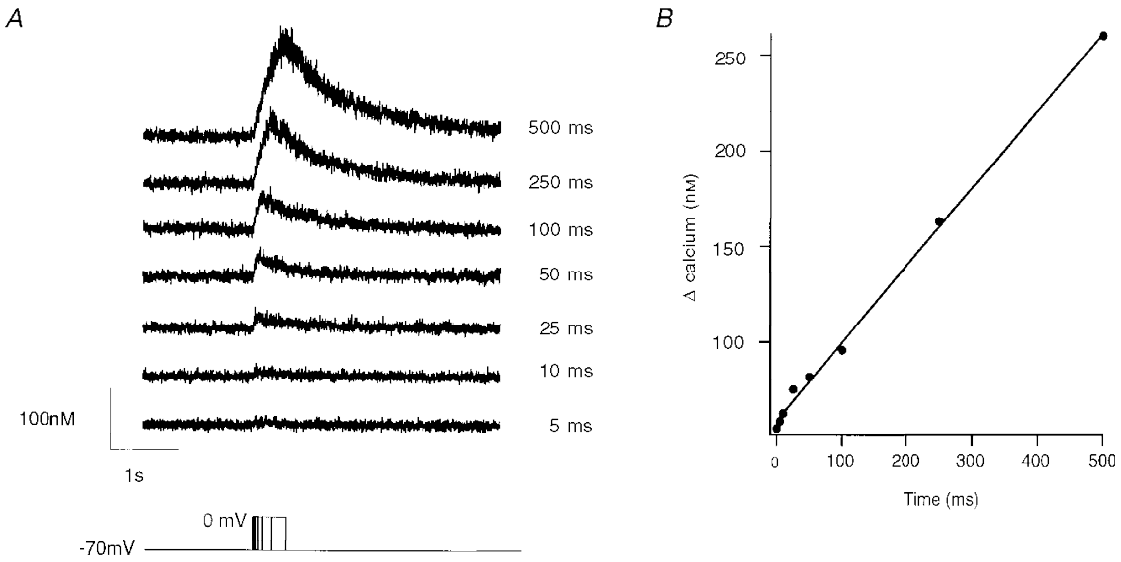

Figure 10. Intracellular calcium transients during depolarizing voltage steps to 0 mV of varying duration

A, calcium measurements associated with voltage steps from a holding potential of −70 mV to 0 mV with variable durations. Time step intervals lasted from 5 to 500 ms as indicated in the bottom trace. *B*, peak calcium elevations were plotted against the time of depolarization. Note the linear correlation between the evoked $[Ca^{2+}]_i$ and the depolarization time.

Homma, 1992; O'Donovan *et al.* 1994; Bacskai *et al.* 1995; Ramirez *et al.* 1996). The combination of infrared differential interference contrast optics (Stuart *et al.* 1993; Dodt & Zieglgänsberger, 1994), whole-cell patch clamp recordings and microfluorimetric techniques applied to the intact respiratory system appears as a powerful approach enabling high resolution current and voltage clamp recordings together with microfluorometric measurements from identified neurones. By performing simultaneous patch clamp and microfluorometric calcium measurements of respiratory neurones in the pre-Bötzinger complex, we were able to monitor intracellular calcium concentrations during ongoing respiratory activity (see also Koshiya & Smith, 1997). Several observations indicated that a defined subpopulation of inspiratory interneurones was analysed in this report. First, rhythmic respiratory activity of neurones was time locked with the inspiratory phase of the hypoglossal nerve, confirming that inspiratory-type

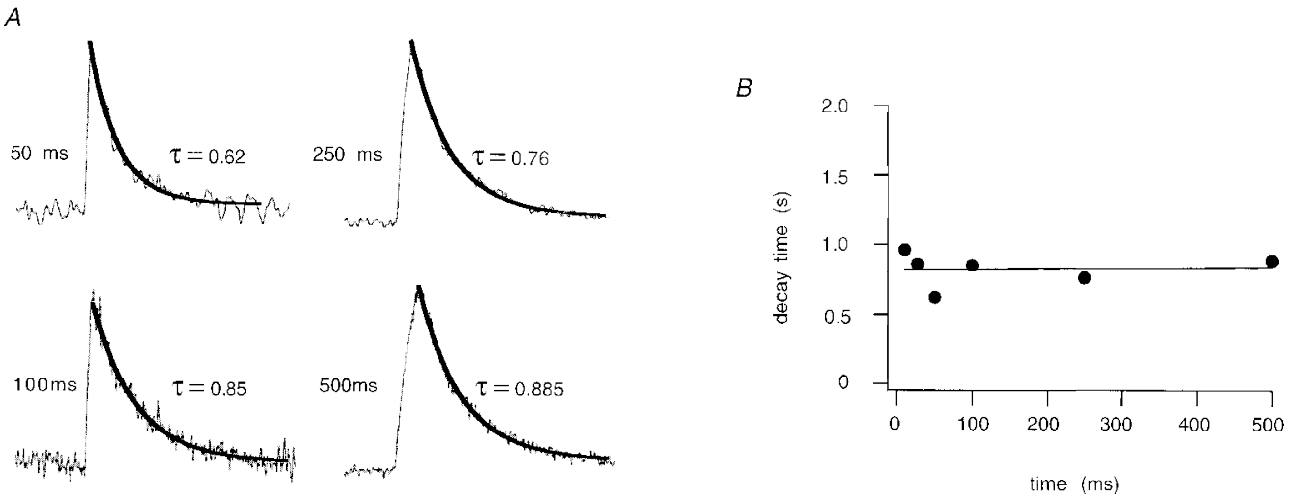

Figure 11. Decay of calcium transients during depolarizing voltage steps

A, normalized calcium elevations elicited by depolarizations to 0 mV with variable durations as indicated in Fig. 9. Single exponential fits are shown for depolarizing pulses of 50, 100, 250 and 500 ms. *B*, in the diagram decay times are plotted as a function of the length of depolarization. Decay times for different $[Ca^{2+}]_i$ were similar.

neurones were investigated (Smith *et al.* 1991; Ramirez *et al.* 1997). Second, their current–voltage relationship displayed a notable outward rectification for membrane potentials positive to −60 mV, separating them functionally from vagal motoneurones characterized by linear current–voltage relationships (see for example Rekling *et al.* 1996; Rekling & Feldman, 1997). Third, input resistances of inspiratory interneurones ranged from 600 to 800 MΩ, which was notably larger than average values of 120 MΩ found for large vagal motoneurones under comparable experimental conditions (Rekling *et al.* 1996; Rekling & Feldman, 1997).

In this study we report rhythmic calcium oscillations in the functionally intact respiratory network. During patch clamp recordings cells were loaded with the calcium indicator dye fura-2 allowing measurements of somatic calcium transients starting within the first seconds after establishing the whole-cell recording configuration. Calcium-dependent and -independent fluorescence signals were integrated over a variable region of interest representing the average calcium signal from one cell soma. Recording conditions were sufficiently stable to perform simultaneous patch clamp and microfluorometric measurements over several hours. Calcium measurements were calibrated for inhomogeneities in dye concentrations by performing ratiometric calcium measurements (Grynkiewicz *et al.* 1985). The remarkable resolution of fluorescence measurements was exemplified by the detection of calcium signals elicited by single action potentials.

In the presence of fura-2 concentrations below 200 μM, spontaneous calcium oscillations in respiratory neurones displayed amplitudes around 300 nM and decay time constants of 1·6 s (28 °C). Both parameters notably depend on the experimental conditions used for calcium measurements. For example, calcium indicator dyes represent an exogenously added cellular buffer reducing peak concentrations of intracellular free calcium and prolonging their decay times (Neher & Augustine, 1992; Neher, 1995; Helmchen *et al.* 1996; Lips & Keller, 1998). To approximate calcium kinetics under physiological conditions, we measured calcium decay time constants directly after establishing the whole-cell configuration. In this case, only small amounts of fura-2 had diffused into the cell presumably representing undisturbed buffering conditions (Neher, 1995). From such experiments, calcium transients with exponential decay time constants of several hundred milliseconds were extrapolated for dye-free conditions, suggesting notably shorter time constants for *in vivo* kinetics at 37 °C. For a more detailed analysis, it is necessary to perform a systematic study investigating defined calcium transients with different buffer types and varying buffer concentrations (see for example Neher, 1995; Helmchen *et al.* 1996; Lips & Keller, 1998), which is an interesting area for future investigation.

Several observations indicated that calcium influx through voltage-regulated calcium channels (Carbone & Lux, 1987; Onimaru & Homma, 1992; Pierrefiche *et al.* 1996*a*, *b*; Elsen & Ramirez, 1997) was a major source for calcium oscillations in respiratory neurones. Firstly, the strong correlation between membrane depolarization and calcium elevation indicated the involvement of voltage-activated calcium influx. Secondly, the absence of calcium oscillations in voltage clamp measurements was well explained by the closure of voltage-dependent calcium channels at hyperpolarizing voltages (Carbone & Lux, 1987). Thirdly, rise times of 150 ms suggested that the rapid calcium influx rates characteristic of the opening of ion channels shaped the onset of somatic $[Ca^{2+}]_i$. Voltage clamp analysis of calcium influx pathways clearly demonstrated voltage-dependent Ca^{2+} channels in respiratory neurones that opened for membrane depolarizations to voltages more positive than −55 mV. These data showed that moderate depolarizations underlying periodic bursts of inspiratory synaptic activity could lead to notable calcium influx into the soma. This was in agreement with earlier electrophysiological measurements suggesting a prominent role of Ca^{2+}-activated potassium conductances in modulation of respiratory bursts and repolarizaton of respiratory neurones after bursts of action potential discharges (Richter *et al.* 1993; Pierrefiche *et al.* 1995). The molecular identification of influx pathways, i.e. the involvement of non-selective cation channels (Partridge & Swandulla, 1988), different types of ligand-gated cation channels (Foutz *et al.* 1989; Greer *et al.* 1991; Keller *et al.* 1992; Weigand & Keller, 1998) or voltage-regulated calcium channels (Carbone & Lux, 1987; Richter *et al.* 1993; Pierrefiche *et al.* 1995; Onimaru *et al.* 1996) will require further experiments involving a detailed pharmacological, electrophysiological and spatial analysis of calcium fluxes.

Microfluorometric calcium measurements showed that essentially high voltage-activated calcium channels mediated the dominant contribution to somatic calcium responses of respiratory neurones in the rhythmically active preparation. Although LVA channels have been shown to exist in respiratory neurones (Onimaru *et al.* 1996), their contribution to somatic calcium concentrations appeared to be relatively small under our experimental conditions. One explanation could be that LVA channels were primarily located in dendrites so that their contribution to intracellular calcium profiles remained undetected during somatic measurements. This is consistent with the observation that large negative currents had to be injected into the soma to fully de-inactivate LVA calcium currents during *in vivo* experiments (Pierrefiche *et al.* 1996*b*). Another explanation might be that neurones of relatively young animals investigated in this report (2–8 days) displayed low expression of LVA channels in this stage of development. Interestingly, we found little or no evidence for a significant contribution of calcium-induced calcium release (CICR) to spontaneous calcium oscillations under our experimental conditions (Neher & Augustine, 1992; Llano *et al.* 1994). This was not surprising as relatively low elevations of $[Ca^{2+}]_i$ during rhythmic activity might not be sufficient to induce substantial calcium release (O'Sullivan *et al.* 1989;

Llano *et al.* 1994; Yuste & Tank, 1996). It is interesting to note, however, that our observations do not rule out the possibility that magnified calcium amplitudes under dye-free *in vivo* conditions might still be sufficient to trigger intracellular calcium release events.

Calcium extrusion mechanisms in respiratory neurones were investigated by monitoring decays of calcium signals as a function of calcium elevations. For concentrations below 1 μM, calcium decays were well described by a single exponential function and the decay time constant was independent of maximal amplitude, suggesting that calcium extrusion was readily described by a linear kinetic scheme with no or little calcium dependence of transition rates. An interesting observation in our measurements was the notable heterogeneity of intracellular calcium signals during ongoing rhythmic activity. One explanation might be the variance of discharge frequency of action potentials within a burst, which were well correlated with amplitudes of calcium signals. Another factor that could have affected the time course of calcium transients was the gradual perfusion of the cytosol with pipette solutions, which could have resulted in a progressive modification of 'endogenous' calcium dynamics after establishing the whole-cell configuration.

With respect to the overall function of the respiratory network, several conclusions can be drawn from the simultaneous electrophysiological and fluorimetric calcium measurements. Firstly, membrane depolarization was a necessary condition for spontaneously occurring, rhythmic elevations in somatic $[Ca^{2+}]_i$. Secondly the absence of calcium transients in voltage clamp mode also indicated that activation of synaptic receptors alone was not sufficient for changes in somatic calcium concentrations. These observations are in good agreement with earlier reports suggesting that rhythmic changes in intracellular calcium concentration play a substantial role in shaping respiratory activity (Richter *et al.* 1993; Pierrefiche *et al.* 1995). Subsequent oscillations in the activity of calcium-dependent second messenger systems or conductances might form an elementary link to mechanisms of activity-dependent adjustment of rhythmic activity in central neurones. For future investigations, one particular interesting aspect relates to the concept that second messenger systems are dynamically adjusted to rhythmic activity essential for physiological and pathophysiological states of the central nervous system.

Bacskai, B. J., Wallen, P., Lev Ram, V., Grillner, S. & Tsien, R. Y. (1995). Activity-related calcium dynamics in lamprey motoneurons as revealed by video-rate confocal microscopy. *Neuron* **14**, 19–28.

Bertolino, M. & Llinas, R. R. (1992). The central role of voltage-activated and receptor-operated calcium channels in neuronal cells. *Annual Review of Pharmacology and Toxicology* **32**, 399–421.

Bianchi, A. L., Denavit-Saubie, M. & Champagnat, J. (1995). Central control of breathing in mammals: neuronal circuitry, membrane properties, and neurotransmitters. *Physiological Reviews* **75**, 1–45.

Bootman, M. D., Berridge, M. J. & Lipp, P. (1997). Cooking with calcium: the recipes for composing global signals from elementary events. *Cell* **91**, 367–373.

Carbone, E. & Lux, H. D. (1987). Kinetics and selectivity of a low-voltage-activated calcium current in chick and rat sensory neurons. *Journal of Physiology* **386**, 547–570.

Champagnat, J. & Richter, D. W. (1993). Second messenger-induced modulation of the excitability of respiratory neurons. *NeuroReport* **4**, 861–863.

Champagnat, J. & Richter, D. W. (1994). The roles of K^+ conductance in expiratory pattern generation in anaesthetized cats. *Journal of Physiology* **479**, 127–138.

Dodt, H. U. & Zieglgänsberger, W. (1994). Infrared videomicroscopy: a new look at neuronal structure and function. *Trends in Neurosciences* **17**, 453–458.

Edwards, F., Konnerth, A., Sakmann, B. & Takahashi, T. (1989). A thin slice preparation for patch clamp recordings from neurones of the mammalian central nervous system. *Pflügers Archiv* **414**, 600–612.

Elsen, F. P. & Ramirez, J. M. (1997). Hypoxia reduces the amplitude of voltage-dependent calcium currents in the isolated respiratory system of mice. *Society for Neuroscience Abstracts* **23**, 495.11.

Fierro, L. & Llano, I. (1996). High endogenous calcium buffering in Purkinje cells from rat cerebellar slices. *Journal of Physiology* **496**, 617–625.

Foutz, A. S., Champagnat, J. & Denavit, S. M. (1989). Involvement of N-methyl-D-aspartate (NMDA) receptors in respiratory rhythmogenesis. *Brain Research* **500**, 199–208.

Frermann, D., Keller, B. U. & Richter, D. W. (1997*a*). Intracellular calcium oscillations in spontaneously active respiratory neurons of mouse. *Pflügers Archiv* **433**, R 97.

Frermann, D., Keller, B. U. & Richter, D. W. (1997*b*). Intracellular calcium oscillations in spontaneously active respiratory neurons of mouse. *Society for Neuroscience Abstracts* **23**, 495.9.

Funk, G. D., Smith, J. F. & Feldman, J. L. (1993). Generation and transmission of respiratory oscillations in medullary slices: role of excitatory amino acids. *Journal of Neurophysiology* **70**, 1497–1515.

Greer, J. J., Smith, J. C. & Feldman, J. L. (1991). Role of excitatory amino acids in the generation and transmission of respiratory drive in neonatal rat. *Journal of Physiology* **437**, 727–749.

Grynkiewicz, G., Poenie, M. & Tsien, R. Y. (1985). A new generation of Ca^{2+} indicators with greatly improved fluorescence properties. *Journal of Biological Chemistry* **260**, 3440–3450.

Hamill, O. P., Marty, A., Neher, E., Sakmann, B. & Sigworth, F. J. (1981). Improved patch-clamp techniques for high-resolution current recording from cells and cell-free membrane patches. *Pflügers Archiv* **391**, 85–100.

Helmchen, F., Borst, J. G. & Sakmann, B. (1997). Calcium dynamics associated with a single action potential in a CNS presynaptic terminal. *Biophysical Journal* **72**, 1458–1471.

Helmchen, F., Imoto, K. & Sakmann, B. (1996). Ca^{2+} buffering and action potential-evoked Ca^{2+} signalling in dendrites of pyramidal neurons. *Biophysical Journal* **70**, 1069–1081.

Keller, B. U., Hollmann, M., Heinemann, S. & Konnerth, A. (1992). Calcium influx through subunits GluR1/GluR3 of kainate/AMPA receptor channels is regulated by cAMP dependent protein kinase. *EMBO Journal* **11**, 891–896.

Keller, B. U., Konnerth, A. & Yaari, Y. (1991). Patch clamp analysis of excitatory synaptic currents in granule cells of rat hippocampus. *Journal of Physiology* **435**, 275–293.

Koshiya, N. & Smith, J. C. (1997). Real-time functional and structural imaging of rhythmically active respiratory neurons with calcium-sensitive dyes and IR-DIC medullary slices *in vitro*. *Society for Neuroscience Abstracts* **23**, 495.2.

Lips, M. & Keller, B. U. (1998). Endogenous calcium buffering in motoneurones of the nucleus hypoglossus from mouse. *Journal of Physiology* **511**, 105–117.

Llano, I., DiPolo, R. & Marty, A. (1994). Calcium-induced calcium release in cerebellar Purkinje cells. *Neuron* **12**, 663–673.

Neher, E. (1995). The use of fura-2 for estimating Ca buffers and Ca fluxes. *Neuropharmacology* **34**, 1423–1442

Neher, E. & Augustine, G. J. (1992). Calcium gradients and buffers in bovine chromaffin cells. *Journal of Physiology* **450**, 273–301

O'Donovan, M., Ho, S. & Yee, W. (1994). Calcium imaging of rhythmic network activity in the developing spinal cord of the chick embryo. *Journal of Neuroscience* **14**, 6345–6369.

Onimaru, H., Ballanyi, K. & Richter, D. W. (1996). Calcium-dependent responses in neurons of the isolated respiratory network of newborn rats. *Journal of Physiology* **491**, 677–695.

Onimaru, H. & Homma, I. (1992). Whole cell recordings from respiratory neurons in the medulla of brainstem-spinal cord preparations isolated from newborn rats. *Pflügers Archiv* **420**, 399–406.

O'Sullivan, A. J., Cheek, T. R., Moreton, R. B., Berridge, M. J. & Burgoyne, R. D. (1989). Localization and heterogeneity of agonist-induced changes in cytosolic calcium concentration in single bovine adrenal chromaffin cells from video imaging of fura-2. *EMBO Journal* **8**, 401–411.

Partridge, L. D. & Swandulla, D. (1988). Calcium-activated non-specific cation channels. *Trends in Neurosciences* **11**, 69–72.

Penner, R., Fasolato, C. & Hoth, M. (1993). Calcium influx and its control by calcium release. *Current Opinion in Neurobiology* **3**, 368–374.

Pierrefiche, O., Champagnat, J. & Richter, D. W. (1995). Calcium-dependent conductances control neurons involved in termination of inspiration in cats. *Neuroscience Letters* **184**, 101–104.

Pierrefiche, O., Haji, A. & Richter, D. W. (1996*a*). Calcium currents in respiratory neurons *in vivo*. *Pflügers Archiv* **431**, R 91.

Pierrefiche, O., Haji, A. & Richter, D. W. (1996*b*). *In vivo* analysis of voltage-dependent Ca^{2+} currents contributing to respiratory bursting. *Society for Neuroscience Abstracts* **22**, 689.6.

Pietrobon, D., Di Virgilio, F. & Pozzan, T. (1990). Structural and functional aspects of calcium homeostasis in eukaryotic cells. *European Journal of Biochemistry* **193**, 599–622.

Ramirez, J. M., Quellmalz, U. J. & Richter, D. W. (1996). Postnatal changes in the mammalian respiratory network as revealed by the transverse brainstem slice of mice. *Journal of Physiology* **491**, 799–812.

Ramirez, J. M., Telgkamp, P., Elsen, F. P. & Richter, D. W. (1997). Respiratory rhythm generation in mammals: synaptic and membrane properties. *Respiratory Physiology* **110**, 71–85.

Rekling, J. C., Champagnat, J. & Denavit-Saubie, M. (1996). Thyrotropin-releasing hormone (TRH) depolarizes a subset of inspiratory neurons in the newborn mouse brain stem *in vitro*. *Journal of Neurophysiology* **75**, 811–819.

Rekling, J. C. & Feldman, J. L. (1997). Bidirectional electrical coupling between inspiratory motoneurons in the newborn mouse nucleus ambiguus. *Journal of Neurophysiology* **78**, 3508–3510.

Richter, D. W., Ballanyi, K. & Schwarzacher, S. (1992). Mechanisms of respiratory rhythm generation. *Current Opinion in Neurobiology* **2**, 788–793.

Richter, D. W., Champagnat, J., Jacquin, T. & Benacka, R. (1993). Calcium currents and calcium-dependent potassium currents in mammalian medullary respiratory neurons. *Journal of Physiology* **470**, 23–33.

Sakmann, B., Edwards, F., Konnerth, A. & Takahashi, T. (1989). Patch clamp techniques used for studying synaptic transmission in slices of mammalian brain. *Quarterly Journal of Experimental Physiology* **74**, 1107–1118.

Schneggenburger, R., Zhou, Z., Konnerth, A. & Neher, E. (1993). Fractional contribution of calcium to the cation current through glutamate receptor channels. *Neuron* **11**, 133–143.

Smith, J. C., Ballanyi, K. & Richter, D. W. (1992). Whole-cell patch-clamp recordings from respiratory neurons in neonatal rat brainstem in vitro. *Neuroscience Letters* **134**, 153–156.

Smith, J. C., Ellenberger, H. H., Ballanyi, K., Richter, D. W. & Feldman, J. L. (1991). Pre-Bötzinger complex: a brainstem region that may generate respiratory rhythm in mammals. *Science* **254**, 726–729.

Stuart, G. J., Dodt, H. U. & Sakmann, B. (1993). Patch-clamp recordings from the soma and dendrites of neurons in brain slices using infrared video microscopy. *Pflügers Archiv* **423**, 511–518.

Titz, S. & Keller, B, U. (1997). Rapidly deactivating AMPA receptors determine excitatory synaptic transmission to interneurons in the nucleus tractus solitarius from rat. *Journal of Neurophysiology* **78**, 82–91.

Tsien, R. W. & Tsien, R. Y. (1990). Calcium channels, stores and oscillation. *Annual Review of Cell Biology* **6**, 715–760.

Viana, F., Bayliss, D. A. & Berger, A. J. (1993). Calcium conductances and their role in the firing behavior of neonatal rat hypoglossal motoneurons. *Journal of Neurophysiology* **69**, 2137–2149.

Weigand, E. & Keller, B. U. (1998). Functional diversity of synaptic AMPA/KA receptor channels as revealed by subtype-specific antagonists. *European Journal of Neuroscience* **10**, 64–70.

Yuste, R. & Tank, D. W. (1996). Dendritic integration in mammalian neurons, a century after Cajal. *Neuron* **16**, 701–716.

Zhou, Z. & Neher, E. (1993). Mobile and immobile calcium buffers in bovine adrenal chromaffin cells. *Journal of Physiology* **469**, 245–273.

Acknowledgements

We thank D. Crzan and U. Lange for technical assistance and S. Titz and P. Lalley for valuable comments on the manuscript. This research was supported by grant Ke 403/6-1 to B.K., the Sonderforschungsbereich 406 and the Graduiertenkolleg 'Organisation and Dynamics of Neuronal Nets'.

Corresponding author

B. U. Keller: Zentrum Physiologie, Humboldtallee 23, 37073 Göttingen, Germany.

Email: bkeller@neuro-physiol.med.uni-goettingen.de